Pergamon

Int. J. Heat Mass Transfer. Vol. 37, Suppl. 1, pp. 311–324, 1994

0017-9310/94 $6.00 + 0.00

0017-9310(93)E0064-N

Spectral radiative properties identification of fiber insulating materials

V. P. NICOLAU,† M. RAYNAUD and J. F. SACADURA

Centre de Thermique-URA CNRS 1372, Institut National des Sciences Appliquées de Lyon, 69621, Villeurbanne cedex, France

Abstract—Particulate media, among which some are porous, like fibers, powders, foams and others, are of considerable interest in many engineering applications. Heat transfer in such media is due to complex mechanisms involving interactions of radiation with conduction and/or convection. Improvements of the thermal performance of these materials, used, for instance, for thermal insulation, need a good understanding of the physical phenomena involved, combined to an accurate knowledge of the thermophysical properties responsible for these performances. This paper deals with the determination of the spectral properties: optical thickness, albedo and phase function shape parameters, that govern the radiative transfer in a semi-transparent medium. Results are presented for fiberglass and silica fibers–cellulose insulations.

1. INTRODUCTION

HEAT TRANSFER by combined conduction or convection with radiation through a participating medium capable of absorbing, emitting and scattering thermal radiation is a problem of great practical importance. This situation is well illustrated by high porosity materials widely used in many industrial high technology applications and in building insulation. Although analytical or numerical techniques are available for solving the coupled heat transfer problem, results are still uncertain because of the lack of well known spectral radiative properties. Various approaches to determine radiative properties have been employed by several researchers. Many papers were recently reviewed by McCormick [1] and by Petrov [2]. A brief literature survey shows two distinct approaches: (i) analytical determination of individual cylindrical or spherical particle radiative properties (Mie and Kerker theories) and a generalization accounting for the morphology of the medium; (ii) experimental transmittance and reflectance determination through an inversion of the radiative transfer equation to obtain the medium properties. The first approach frequently includes an experimental validation.

The work of Lee [3] is a typical example of the first approach. It presents a formulation and an evaluation of the effective phase function for fibrous media with any particulary kind of fiber orientation or whose fibers are randomly oriented in space. Banner *et al.* [4] presented a study on the temperature dependence on the optical characteristics (complex index of refraction) of the original solid material. The radiative characteristics, as extinction and backscattering coefficients and albedo, are obtained for the fibrous media. The calculated heat flux is compared with measurements performed in a guarded hot plate apparatus. The work of Jeandel *et al.* [5], focuses on radiative transfer for a layer of silica fibers with random azimuthal orientation. The theory of scattering from an individual fiber is used to obtain the absorption, extinction and backscattering coefficients. Using the two-flux model, a radiative conductivity is calculated. Then, the effects of the fiber diameter on this radiative conductivity are analysed. Finally an experimental validation on normal transmittance measurements is done with a spectrometer.

Using the second approach, Yeh and Roux [6], have measured hemispherical reflectance of commercial fiberglass. The samples are placed on an Al foil. A FTIR spectrometer coupled to an integrating sphere allows the wavelength range from 4 to 19 μm to be covered. The radiative transfer equation is solved using the discrete ordinates method; its inversion allows us to determine the absorption and scattering coefficients. Isotropic and anisotropic phase function models are taken into account. Some results of the extinction coefficient, for the 20–80 μm wavelength range, are also obtained applying Beer's law to specular reflectance data. Glicksman *et al.* [7] described a technique for the determination of the extinction coefficient, the albedo and the phase function values for foams and fiberglass. The extinction coefficient is calculated using Beer's law. Neglecting the secondary scattering (only the primary scattering from an incident laser beam is considered), a simplified solution of the radiative transfer equation allows us to obtain the albedo and phase function product in each measurement direction. Then, the normalization of

† Permanent address: Mechanical Engineering Department, UFSC 88049, Florianópolis, SC, Brazil.

NOMENCLATURE

A_j jth Gauss quadrature weight
C_j jth Gauss quadrature coefficient
CN condition number
$d\omega_d$ solid angle of the detected radiation [sr^{-1}]
$d\omega_o$ solid angle of the collimated incident radiation [sr^{-1}]
F sum of the square errors, equation (10)
f_1 weighting factor between forward and backward anisotropy in the phase function
f_2 weighting factor between anisotropic and isotropic scattering
g anisotropy factor in the Henyey–Greenstein phase function
g_1 equal to g, in the forward direction
g_2 equal to g, in the backward direction
I spectral radiative intensity [$W\,m^{-3}\,sr^{-1}$]
I_c spectral collimated radiation intensity [$W\,m^{-3}\,sr^{-1}$]
I_s spectral scattered radiation intensity [$W\,m^{-3}\,sr^{-1}$]
I^o spectral blackbody radiation intensity [$W\,m^{-3}\,sr^{-1}$]
I_o spectral collimated radiation intensity incident onto the sample [$W\,m^{-3}\,sr^{-1}$]
N number of measurement directions
p phase function
T_t theoretical transmittance or reflectance value [sr^{-1}] directional
T_e experimental transmittance or reflectance value [sr^{-1}] directional.

Greek symbols
β_j any of the six parameters involved in the initial inverse problem
θ polar angle
θ_o polar angle of divergence of the collimated incident beam
μ $\cos\theta$
τ optical coordinate
τ_o sample's optical thickness
ω albedo = scattering to extinction coefficient ratio.

the phase function is used to separate both values from this product. The experimental set-up includes a CO_2 laser (9.64 μm) and a bidirectional transmittance–reflectance apparatus. Finally a weighted scattering coefficient is calculated in order to use the diffusion approximation (Rosseland equation) in heat transfer problems.

Kamiuto *et al.* [8–10] and Kamiuto [11] have presented a series of papers dealing with the optical thickness, albedo and the phase function identification. Henyey–Greenstein phase function model, with an asymmetry factor g, is adopted. The optical thickness is calculated directly using Beer's law, applied to the collimated beam incident onto to sample. In such a case, scattering in the normal direction is estimated using transmittance data in the neighboring region. Albedo and g factor are identified by an inverse method. Sample materials studied are cordierite, porous Ni–Cr plates [8], packed-spheres [9, 10], or packed-spheres bounded by transparent plates [11]. A bidirectional transmittance/reflectance apparatus is employed using a He–Ne laser (0.63 μm) as a radiation source and a photo-multiplier tube as a detector.

Kuhn *et al.* [12] determined the scaled albedo and the mass specific extinction coefficient solving the radiation transfer equation with a 3-flux model. The samples analysed are powders placed on an horizontal film. A FTIR-spectrometer is used. The dependence of powder concentration on the extinction coefficient is shown. A dependent scattering is considered and corrections are adopted to account for such a dependence.

Sacadura *et al.* [13], Uny [14], Sacadura and Nicolau [15] and Doumenc [16], used an ordinary prism spectrometer to measure transmittances and reflectances of fiberglass and carbon foam samples. An inverse method based on the Hooke and Jeeves minimization algorithm allows the extinction coefficient, the albedo and an one-parameter phase function to be obtained.

In this work, the experimental set-up presented in refs. [13–16] is used to perform measurements on fiberglass and silica fiber–cellulose samples in the 1–5 μm wavelength range. First of all a description of the experimental set-up is done, followed by the presentation of the theoretical model employed. Discretizations and other main features of the model solution are also presented. A sensitivity analysis is performed on a 6-parameter model, including optical thickness, albedo and a 4-parameter phase function. A condition number is introduced in order to simplify the parameter linear dependence analysis. Finally a direct method for optical thickness determination is discussed and some results for two fibrous materials are presented.

2. EXPERIMENTAL SET-UP

The experimental set-up shown in Fig. 1 allows the measurement of the incident radiation flux and of the radiation transmitted or reflected by the sample in different directions.

A Pyrox® furnace, reaching 1600°C, is used as a blackbody source. The radiation emitted from a small hole drilled through the furnace wall falls onto a spherical mirror and is reflected onto the mono-

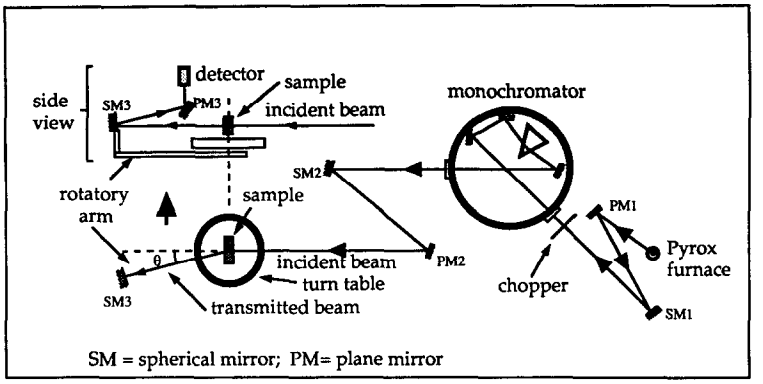

FIG. 1. Experimental set-up.

chromator entrance slit. The monochromator used is a NaCl prism model. A chopper disk modulates the beam before the monochromator. The monochromator exit slit selects a specific beam of wavelength λ, with a $\Delta\lambda$ spectral resolution given by the prism and the slit width used. This radiation is reflected by a spherical mirror SM2, focused on the exit slit. Therefore, the reflected radiation forms a beam of nearly-parallel rays, with a divergence of half-angle θ_o, depending on the exit slit aperture and on the SM2 focal distance. This is the radiation incident onto the sample. The beam issued from the sample and detected is also a nearly-parallel beam, with a divergence of half-angle θ_d, depending on the detector sensitive area radius and on the SM3 mirror focal distance. It is important to notice that, for a correct measurement of the radiation intensity in the direction normal to the sample (scattered and collimated radiation), a detection half-angle θ_d, smaller than the collimated half-angle θ_o, must be used. The third spherical mirror SM3, focusing onto the detector cell, is used to concentrate the beam onto the detector. An InSb detector mounted on a rotating arm allows the measurement of the radiation transmitted or reflected by the sample at several angles. The sample mounting system includes a diaphragm used to limit the transmitted, reflected and incident radiation beams.

The experimental bidirectional transmittance $T_c(\theta)$ for normal incident radiation is defined by the following expression:

$$T_c(\theta) = \frac{I(\theta)}{I_o \, d\omega_o} \tag{1}$$

where I is the transmitted or reflected intensity and I_o, the intensity of the collimated beam normally incident onto the sample within a solid angle $d\omega_o$. Thus $I_o \, d\omega_o$ represents the incident radiation flux. This experimental set-up gives the transmittance data for different angles. The objective of this study is to determine the radiative properties of a sample which minimize the square of the differences between measured and calculated transmittances.

3. ANALYSIS

The design of the experimental set-up is such that the radiative transfer in the sample is one dimensional with azimuthal isotropy (case of incident radiation normal to the sample). The radiation transfer equation (RTE), for a plane slab of a cold semi-transparent medium, with azimuthal isotropy can be written in the following form:

$$\mu \frac{dI_\nu(\tau_\nu,\mu)}{d\tau_\nu} = -I_\nu(\tau_\nu,\mu) + \frac{\omega_\nu}{2} \int_{-1}^{+1} p_\nu(\mu',\mu) I_\nu(\tau_\nu,\mu') \, d\mu' \tag{2}$$

where $\mu = \cos\theta$; θ is the polar angle; I_ν is the spectral intensity of radiation; $\tau_\nu = \beta_\nu x$, $\beta_\nu = \kappa_\nu + \sigma_\nu$ where β_ν, κ_ν, and σ_ν are the spectral volumetric extinction, absorption and scattering coefficients, respectively, and x is a geometrical coordinate. The medium is characterized by the following spectral radiative properties: the optical thickness $\tau_{o\nu} = \beta_\nu L$, where L is the geometrical thickness of the slab, the albedo ω_ν, which is the ratio between the scattered and extincted radiation, and the scattering phase function $p_\nu(\mu', \mu)$. The subscript (ν) denotes a spectral quantity.

In the RTE the radiation intensity in the medium decreases due to the absorption and out-scattering and increases due to in-scattering. The emission term is not considered in the RTE because the experiment uses a modulated radiation incident onto the sample, combined to a phase sensitive detection technique. So the detected flux is modulated and only the radiation transmitted or backscattered by the sample is measured.

The choice of the phase function representation is a critical problem. A classical approach consists of developing this function in a limited series of Legendre polynomials. This approach may lead, in the case of some particulate media like fibers or foams, to very high order developments and, subsequently may require the determination of a large number of coefficients. An alternative solution proposed by

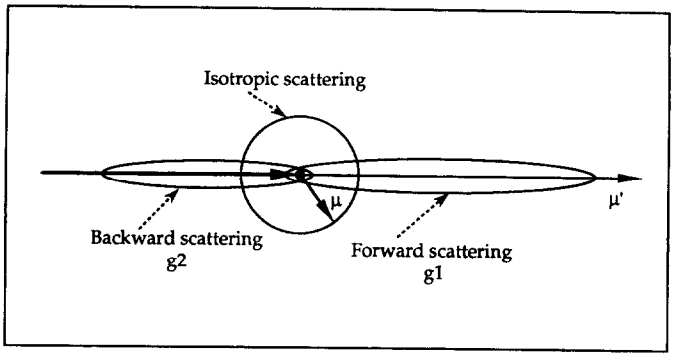

FIG. 2. Phase function composition.

Henyey and Greenstein (H–G) consists in representing the phase function by the following function [14]:

$$p_{\mathrm{HG},g}(\mu',\mu) = \frac{1}{2\pi}\int_0^{2\pi} \times \frac{(1-g^2)\,\mathrm{d}\phi}{[1+g^2-2g(\mu'\mu+\sqrt{(1-\mu'^2)}\sqrt{(1-\mu^2)}\cos\phi)]^{3/2}}. \quad (3)$$

In this function ϕ is the azimuthal angle which disappears once the integration is done; g is the parameter which governs the anisotropy of scattering. It varies from 0 for isotropic scattering, to 1 or -1 for forward or backward scattering, respectively. So, in respect to the parameter identification aims, the H–G function, which requires only one form parameter to be determined, seems to be an attractive approach [13]. However, in a previous work [15], the authors have shown that a unique H–G function is not an appropriate representation of scattering distribution for fiber or foam media, due to the simultaneous presence of highly forward peaked scattering combined to a fair back-scattering, which is observed for this kind of material.

Thus, in the current work, an attempt has been made to better represent the phase function by using a combination of two H–G functions coupled with an isotropic component:

$$p_v(\mu',\mu) = f_1 f_2 p_{\mathrm{HG},g_1}(\mu',\mu) + (1-f_1)f_2 p_{\mathrm{HG},g_2}(\mu',\mu) + (1-f_2). \quad (4)$$

In this expression f_1 and f_2 are two parameters allowing us to weight the participation of the two H–G functions governed by the shape parameters g_1 and g_2, respectively. The constant term $(1-f_2)$ is the isotropic contribution to the phase function. A schematic representation of this combination is shown in Fig. 2. This new model of the phase function implies that four parameters ranging in the interval (0,1) must now be identified: the forward g_1, and backward, g_2, anisotropy parameters and the fraction parameters f_1 and f_2. Figure 3 shows a representation of equation (4) as well as of a single H–G function with the same g_1 coefficient. The values are approximately identical in the forward scattering region, but are quite different in the backward directions, for which only equation (4) is able to represent some back-scattering. Four coefficients in equation (4) are at least necessary to simulate a highly forward peaked scattering, combined to some backward and isotropic scattering. This is why such a phase function has been considered in the present work.

4. DISCRETIZATION

The radiation field is subdivided into a diffuse and a collimated component of spectral intensity I_d and I_c, respectively (in order to simplify the notations, the subscript v is omitted). The collimated component is the remaining quantity of the original incident radiation, after absorption and scattering by the sample. The incident beam, taken normal to the sample surface, is collimated with a small divergence angle θ_o. Accordingly equation (2) is applied for each intensity component.

The governing equation for the collimated intensity $I_c(\tau)$ is the ordinary differential equation:

$$\frac{\mathrm{d}I_c}{\mathrm{d}\tau} = -I_c \quad (5)$$

with the initial condition $I_c(0) = I_o$. I_o, the incident intensity onto the sample, is a measured parameter. The solution is straightforward: $I_c(\tau) = I_o \exp(-\tau)$. Thus the normal theoretical transmittance, for the collimated radiation, T_{tc}, which is the ratio of the collimated output intensity to the incident radiation flux, is:

$$T_{tc}(\tau) = \frac{\mathrm{e}^{-\tau}}{\mathrm{d}\omega_o}. \quad (6)$$

The governing equation for the scattered component of intensity $I_s(\tau,\mu)$ is:

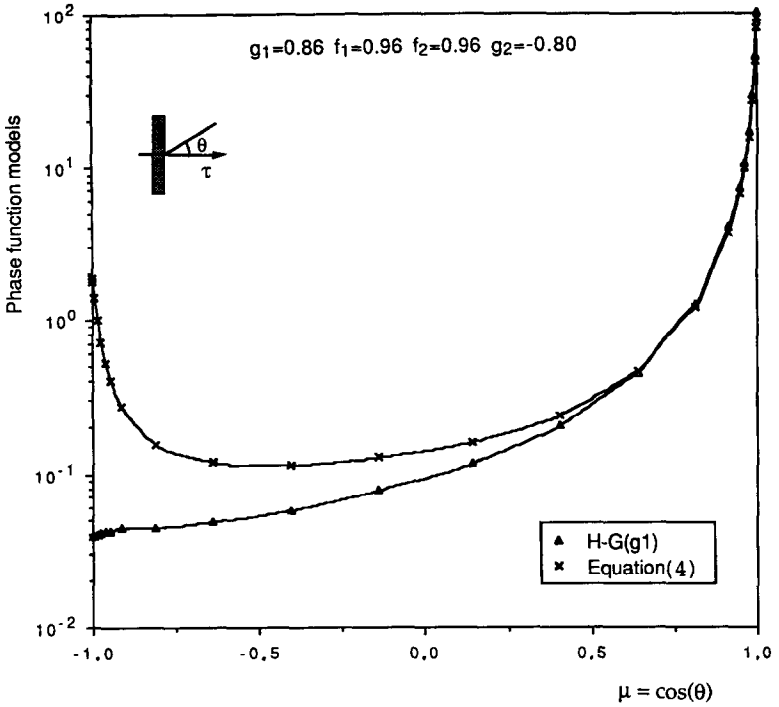

FIG. 3. The four parameters model compared to a Henyey–Greenstein phase function model.

$$\mu\frac{dI_s(\tau,\mu)}{d\tau} = -I_s(\tau,\mu)+\frac{\omega}{2}\int_{-1}^{+1} p(\mu',\mu)I_s(\tau,\mu')\,d\mu' + \frac{\omega}{2}\int_{\mu_o}^{1} p(\mu',\mu)I_c(\tau,\mu')\,d\mu' \quad (7)$$

where $\mu_o = \cos\theta_o$. The boundary conditions are:

$$I_s(0,\mu) = 0, \quad \text{for } \mu > 0 \quad (7a)$$

$$I_s(\tau_o,\mu) = 0, \quad \text{for } \mu < 0. \quad (7b)$$

The set of equations (7) governing the scattered radiation field is solved by the discrete ordinates method which consists of replacing the integrodifferential equations by a system of linear equations. This is carried out through an angular discretization of the intensity field into $2n$ beams in the directions μ_i ($i = \pm 1, \ldots, \pm n$, and $\mu_{-i} = -\mu_i$). It leads to the following set of equations giving the intensity for the $2n$ directions, at any position τ in the medium:

$$\frac{d}{d\tau}[I_s(\tau,\mu)] - [M][I_s(\tau,\mu)] = [K(\tau,\mu)] \quad (8a)$$

where:

$$[I_s(\tau,\mu)] = \begin{bmatrix} I_s(\tau,\mu_1) \\ \cdots \\ I_s(\tau,\mu_n) \\ I_s(\tau,-\mu_1) \\ \cdots \\ I_s(\tau,-\mu_n) \end{bmatrix} \quad (8b)$$

$$[K(\tau,\mu)] = \frac{\omega}{4\pi}e^{-\tau}I_o d\omega_o \begin{bmatrix} p(1,\mu_1)/\mu_1 \\ \cdots \\ p(1,\mu_n)/\mu_n \\ p(1,-\mu_1)/-\mu_1 \\ \cdots \\ p(1,-\mu_n)/-\mu_n \end{bmatrix} \quad (8c)$$

$$[M] = \begin{bmatrix} [A] & [B] \\ -[B] & -[A] \end{bmatrix} \quad (8d)$$

$$A_{ij} = \frac{\omega C_j p(\mu_i,\mu_j)}{2\mu_i} - \frac{\delta_{ij}}{\mu_i} \quad (8e)$$

$$B_{ij} = \frac{\omega C_j p(\mu_i,-\mu_j)}{2\mu_i} \quad (8f)$$

where μ_i is the cosine of discretization direction i and δ_{ij} is the Kronecker symbol. The approximation of the integrals of equation (7) by a finite sum is carried out numerically through a Gauss quadrature. The C_j are the coefficients of the nth order quadrature formula used. The spherical space is discretized into $n = 12$ directions for the positive range of μ and $n = 12$ other symmetric directions for the negative μ. A first region in the interval $0 \leqslant \theta \leqslant \theta_o$ is used for collimated and forward scattering radiation measurements ($\cos\theta_1 = 0°$; $\mu_1 = 1$). It is a unique region containing the original collimated radiation. Beyond this region, a half 10th order Gauss quadrature is used from $\theta = \theta_0$ to 20°, in order to permit a concentration of experimental points in the neighborhood of the normal direction, suitable for forward scattering materials. It

concerns five directions. Finally a half 12th order Gauss quadrature is used from $\theta = 20$ to 90°.

The particular solution of equation (8) is represented in the form $[W]e^{-\tau}$, where $[W]$ is a vector of constant components; its homogeneous solution is obtained through the calculation of the $2n$ eigenvalues λ_j and $2n$ eigenvectors V_j. Therefore, the complete solution for the scattered intensity is:

$$I_s[(\tau,\mu_i)] = \sum_{j=1}^{2n} H_j[V_{ji}]e^{-\lambda_j\tau} + [W_i]e^{-\tau}. \quad (9)$$

The boundary conditions lead to a set of linear equations whose solution provides the values of the constants H_j. Putting $\tau = 0$ or τ_o in the solution gives the intensity of the radiation backscatted or transmitted by the sample, respectively. These solutions divided by $I_o d\omega_o$ provide the bidirectional transmittance, T_{ts}, of the sample in the backward or forward directions. T_{ts} corresponds to the scattered transmittance in the off-normal directions. For the normal direction, the transmittance component relative to the collimated radiation T_{tc}, (equation (6)), must be added. Further details are given in equation (14).

5. PARAMETER IDENTIFICATION METHOD

With the experimental apparatus described in Section 2, a sample of a semi-transparent material can be used in order to determine the experimental transmittances and reflectances, T_{ei}, for several measurement directions θ_i, and a given sample thickness. For the same directions and thickness, the model described above in which the material radiative properties (τ_o, ω, p_v) must be given, is used to calculate the theoretical transmittances and reflectances, T_{ti}. Thus, the objective is to determine the six parameters τ_o, ω, g_1, g_2, f_1 and f_2 which minimize the quadratic error between the measured and calculated transmittances and reflectances over the N measurement directions:

$$F(\tau_o,\omega,g_1,g_2,f_1,f_2) = \sum_{i=1}^{N} [T_{ti}(\tau_o,\omega,g_1,g_2,f_1,f_2) - T_{ei}]^2. \quad (10)$$

Several search methods are available to minimize this function. One consists of drawing contour maps of F vs all of the involved parameters and determining from these maps a set of parameters leading to a minimum of F. This method was used to obtain two parameters, in Kamiuto's work [8]. But it necessarily becomes tedious and uncertain if more parameters are searched. A second way [13–15], is the Hooke–Jeeves method, which is a systematic search method through the addition (or subtraction) of an increment to each involved parameter, until a minimal value of F is reached. This method leads safely to a possible solution, but is not able to detect a poorly-conditioned case, as in the search process, the sensitivity of the model to each parameter is not studied. A third method, used in this work, is the Gauss linearization method [17], which minimizes F by setting to zero the derivatives respect to each of the unknown parameters. At each step of an iterative process, the sensitivity coefficients are calculated and this provides an opportunity to detect possible linear dependences between these coefficients. If it is the case, it is impossible to simultaneously determine all the parameters.

The Gauss linearization method starts by establishing a null derivative of F vs each parameter β_j, $j = 1, \ldots, 6$, to be identified:

$$\frac{\partial F}{\partial \beta_j} = \frac{\partial}{\partial \beta_j}\left[\sum_{i=1}^{N} (T_{ei} - T_{ti}^{k+1})^2\right] = 0; \quad (11)$$

where k denotes the iteration number in the iterative process. The T_{ti}^{k+1} value, at iteration $k+1$, is represented as a function of the k iteration values:

$$T_{ti}^{k+1}(\ldots, \beta_j^k + \Delta\beta_j^{k+1}, \ldots) \cong T_{ti}^k(\ldots,\beta_j^k,\ldots) + \cdots + \left(\frac{\partial T_{ti}}{\partial \beta_j}\right)^k \Delta\beta_j^{k+1} + \cdots. \quad (12)$$

After some algebraic manipulation the following matrix formulation is obtained:

$$\begin{bmatrix} \sum_{i=1}^{N}\left(\frac{\partial T_{ti}}{\partial\beta_1}\right)^2 & \sum_{i=1}^{N}\frac{\partial T_{ti}}{\partial\beta_1}\frac{\partial T_{ti}}{\partial\beta_2} & \cdots & \sum_{i=1}^{N}\frac{\partial T_{ti}}{\partial\beta_1}\frac{\partial T_{ti}}{\partial\beta_6} \\ \sum_{i=1}^{N}\frac{\partial T_{ti}}{\partial\beta_2}\frac{\partial T_{ti}}{\partial\beta_1} & \sum_{i=1}^{N}\left(\frac{\partial T_{ti}}{\partial\beta_2}\right)^2 & \cdots & \sum_{i=1}^{N}\frac{\partial T_{ti}}{\partial\beta_2}\frac{\partial T_{ti}}{\partial\beta_6} \\ \cdots & \cdots & \cdots & \cdots \\ \sum_{i=1}^{N}\frac{\partial T_{ti}}{\partial\beta_6}\frac{\partial T_{ti}}{\partial\beta_1} & \sum_{i=1}^{N}\frac{\partial T_{ti}}{\partial\beta_6}\frac{\partial T_{ti}}{\partial\beta_2} & \cdots & \sum_{i=1}^{N}\left(\frac{\partial T_{ti}}{\partial\beta_6}\right)^2 \end{bmatrix}^k \begin{bmatrix} \Delta\beta_1 \\ \Delta\beta_2 \\ \cdots \\ \Delta\beta_6 \end{bmatrix}^{k+1} = -\begin{bmatrix} \sum_{i=1}^{N}(T_{ti}-T_{ei})\frac{\partial T_{ti}}{\partial\beta_1} \\ \sum_{i=1}^{N}(T_{ti}-T_{ei})\frac{\partial T_{ti}}{\partial\beta_2} \\ \cdots \\ \sum_{i=1}^{N}(T_{ti}-T_{ei})\frac{\partial T_{ti}}{\partial\beta_6} \end{bmatrix}^k. \quad (13)$$

The solution of this system gives the increments $\Delta\beta_j^{k+1}$ to be added to each parameter at each step of the iterative process. The source term, in the right hand side, gives the differences between theoretical and experimental transmittances and reflectances. The matrix on the left hand side is composed of the sensitivity coefficients products, calculated from the theoretical model; it does not directly depend on the experimental values. This matrix can be used in the sensitivity analysis to verify possible linear dependences between the sensitivity coefficients calculated for each parameter. Since the sensitivity coefficients depend on the unknown parameters, the corrections set $\Delta\beta_j$ that is obtained from this equation do not minimize the sum of the squared errors. It is necessary to perform an iterative process, in which at each step, the sensitivity matrix is evaluated, from the updated

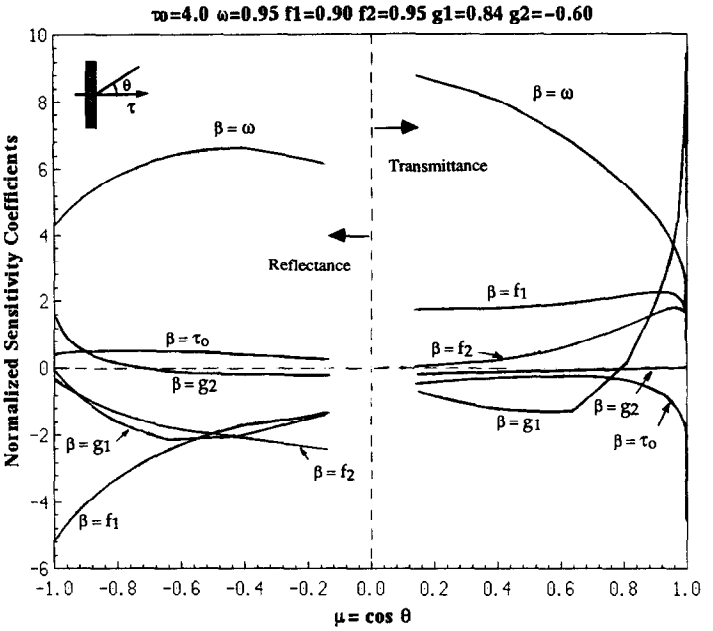

FIG. 4. The normalized sensitivity coefficients for $\tau_o = 4$.

parameter values. The calculation of a condition number of this matrix can be used to determine the degree of ill-posedness of the identification problem. Thus, the sensitivity coefficients are the key of the parameter estimation and must be carefully studied. Rather than looking at the sensitivity coefficient, it is preferable to study the normalized sensitivity coefficients Q_{ij} defined by:

$$Q_{ij} = \frac{\beta_j}{T_{ti}} \frac{\partial T_{ti}}{\partial \beta_j}(\tau_o, \omega, g_1, g_2, f_1, f_2). \tag{14}$$

These normalized coefficients are calculated using back differences with the direct model. They are plotted in Figs. 4 and 5, for $\tau_o = 4$ and 20 (which represent the usual limits of the optical thickness of such samples), and for a selected group of parameter values, vs the angular variable $\mu = \cos\theta$. The calculations were only performed for the 24 angular values that correspond to the measurement angles. The negative μ are for the reflectance and the positive μ for the transmittance. As Fig. 4 shows, the sensitivity of the measurements to τ_o is very weak except for the measurements close to the normal direction ($\theta = 0°$, $\mu = 1$). It means that the measurements far away from the normal are useless for determining τ_o. The sensitivity coefficient for the albedo ω is the largest, thus ω will be the coefficient most accurately determined. g_1, like τ_o, can be estimated only with the measurements close to the normal direction. On the other hand, the sensitivity to f_1 is the largest for reflectance measurements. The sensitivities to f_2 and g_2 are smaller, those of g_2 being almost zero excepted for the backscattering region. This indicates that it will be difficult to estimate g_2.

As the optical thickness is increased up to 20 (Fig. 5), important modifications of the sensitivity coefficients are observed. The stricking point is the nearly linear dependence for the sensitivity coefficients of τ_o, f_1, f_2, g_1 and g_2, which leads to a poorly conditioned system and, as a consequence, to difficulties for simultaneously estimating the six parameters.

The ratio of the normal scattered transmittance to the collimated transmittance, plotted in Fig. 6 as a function of the optical thickness, for two g_1 values, can be used to explain the sensitivity coefficients variations. It shows that the collimated transmittance is much larger when τ_o is small: this is why the optical thickness sensitivity coefficient is large for such τ_o values. When τ_o is greater than 12, the transmittance ratio is larger than 1, thus the normal transmittance is influenced not only by τ_o, but also by f_1, f_2, g_1 and g_2. The sensitivity coefficients indicate that these influences vary very weakly with the angle, consequently the measurements at various angles do not help in estimating simultaneously the five parameters.

After this analysis, it is not yet possible to determine the number of parameters to be identified. Although a linear dependence between two coefficients is not clearly apparent, such a dependence involving three or four parameters is possible, but not readily detectable. In such a case, the condition number CN of the sensitivity matrix $[C]$ (left hand side of equation (13)), must be used [18]:

$$CN(C) = \|C^{-1}\| \cdot \|C\| \tag{15}$$

where the norm $\|C\|$ is calculated from the elements $C_{i,j}$, as:

$$\|C\| = \max_{i=1,6} \sum_{j=1}^{6} C_{i,j}. \tag{16}$$

The condition number is greater than one. The larger the condition number, the worse the ill-conditioning: small changes in the right hand side of equation (13), i.e. in the measurements, result in very large changes in the solution vector, i.e. in the increments $\Delta\beta_j$. It is then almost impossible to simultaneously determine all of the unknown parameters. Poor conditionning occurs when at least two of the sensitivity coefficients are quasi-linearly dependent, or when at least one is very small or very large compared to the others.

In Fig. 7, the condition number is represented as a function of the optical thickness, when several parameters are determined. The six parameter case corresponds to the determination of ω, g_1, f_1, f_2, g_2 and τ_0; the five parameter case to the ω, g_1, f_1, f_2 and g_2 determination, and so on. Obviously, the feasibility of an identification process is strongly dependent on the number of parameters to be identified. Figure 7 shows that the larger the number of parameter, the larger the condition number. There is an exception for the six parameter case, for which the condition number is identical to the five parameter case as long as τ_0 is smaller than 12, and then increases suddenly for larger τ_0. This confirms the information given by the visual study of sensitivity coefficients which showed that simultaneous estimation of the six parameters was very difficult for large optical thickness. This figure also indicates that for any number of parameters, there is one τ_0 optimal interval to perform the identification. If one wants to simultaneously identify the six parameters including τ_0, the optimal value is about 12. But this is not the optimal value to perform the identification of five or less parameters other than τ_0. In such a case the recommended τ_0 value is about 18. This means that it is preferable to identify τ_0 separately from the other parameters.

6. DETERMINATION OF THE OPTICAL THICKNESS

The optical thickness τ_0 (and consequently the extinction coefficient), is an important parameter governing the radiation transfer phenomena. It directly quantifies the radiation attenuation in the medium and must be accurately determined. The previous analysis showed that difficulties will arise for large values of τ_0. Thus, a specific identification procedure has been chosen in order to overcome this problem. It consists of determining τ_0 alone, by a direct method, using only the radiation field in the normal transmission region. This direct determination has already been utilised by Kamiuto [8–11], Doumenc [16] and Glicksman *et al.* [7].

A numerical simulation has been performed to check that this direct method gives accurate enough results. First, the model with the six parameters is used to create a pseudo data set of transmittance measurements. Then, starting from these transmittance data, τ_0 is determined using four different simplified models and the results are compared with the exact value. The first model is simply based on Beer's law [7–16]. The total transmittance in the normal direction is assumed to be equal to the collimated one, which in fact means that multi-scattering in the medium is neglected. The other models, more elaborated, also use Beer's law, but different corrections are applied to extrapolate the scattered transmittance values in the normal direction. This allows the subtraction of the scattered transmittance from the total

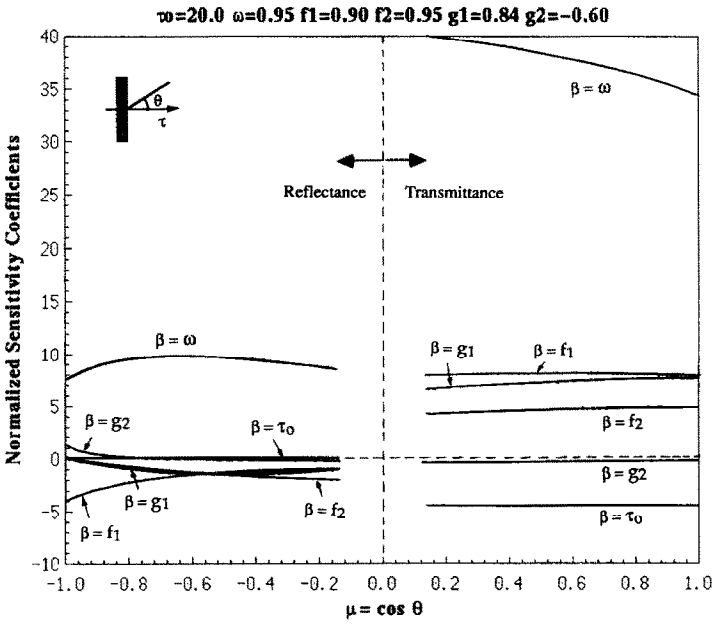

FIG. 5. The normalized sensitivity coefficients for $\tau_0 = 20$.

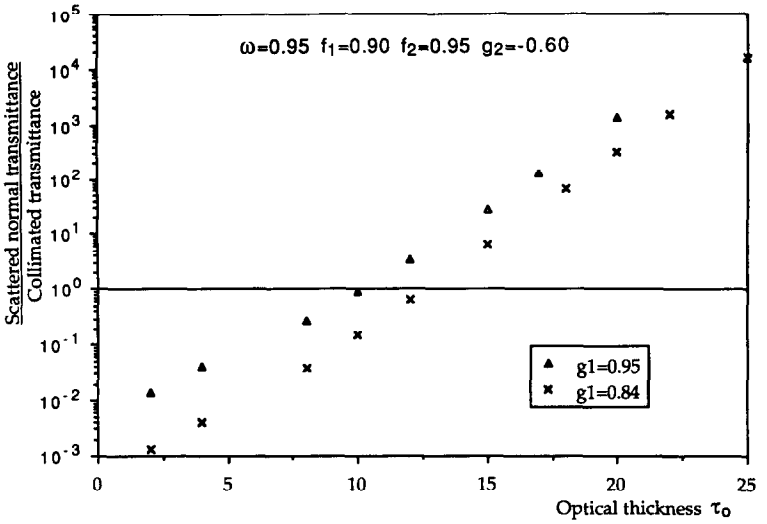

FIG. 6. Normal scattered transmittance to collimated transmittance ratio, from a simulation using equation (9) as model.

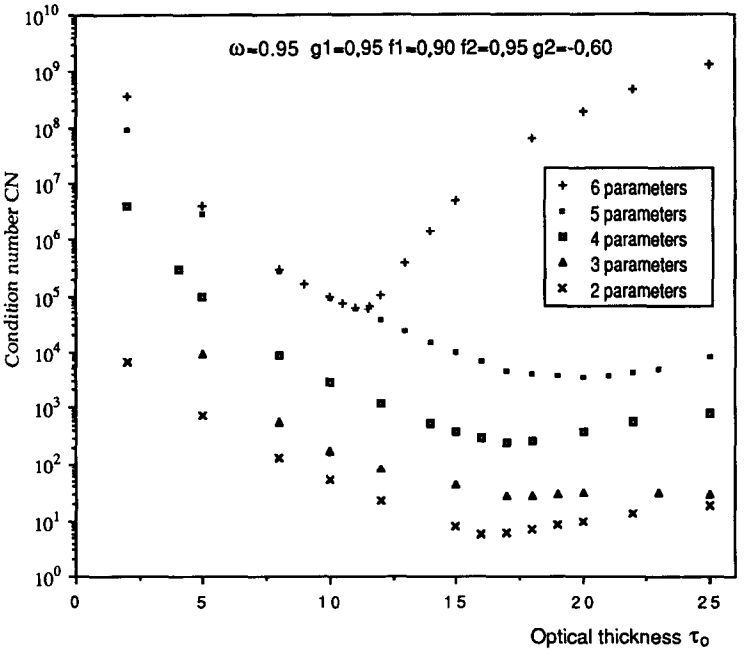

FIG. 7. The condition number, vs τ_o, for a variable number of parameters identification.

transmittance (given by measurement), to obtain a more accurate value of the collimated transmittance. In the so-called 'constant model', it is assumed that the scattered transmittance in the normal direction ($\theta = \theta_1 = 0°$), is equal to the scattered transmittance in the closest measurement direction (θ_2). In the third model, a linear variation of the scattered transmittance is assumed between θ_1 and the normal direction, to extrapolate the scattered radiation to $\theta_1 = 0°$. This linear function is defined from two measurements corresponding to the closest directions (θ_2 and θ_3). Finally, a 'second order' model uses a second order polynomial for the extrapolation. The coefficients of the polynomial are calculated from the scattered transmittance in the two directions (θ_2 and θ_3), and assuming, as a third condition, that the polynomial derivative is zero at $\theta_1 = 0°$.

The ratio of the calculated optical thickness to the reference value, $R\tau_o$, is presented in Fig. 8. A value of unity means that the simplified models are capable to determine the true optical thickness. As we can observe, the Beer's law model gives a poor estimation. This is the consequence of the absence of multi-scattering. The multi-scattering, weak and negligible for

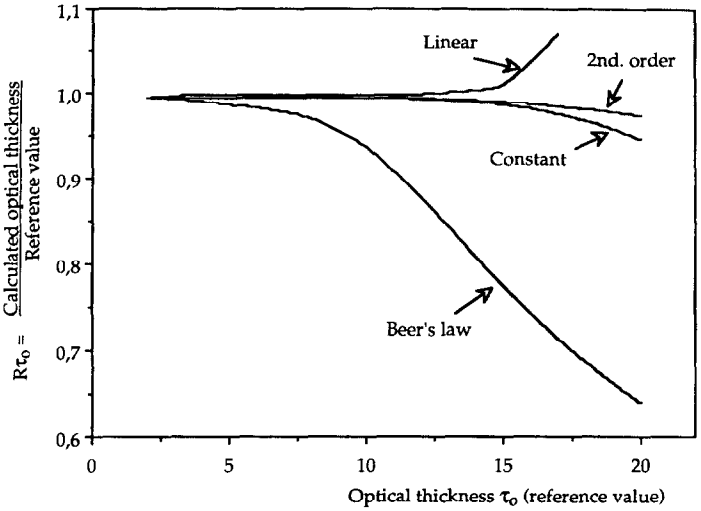

FIG. 8. Optical thickness ratio for different models. (Reference simulation using $\omega = 0.95$; $g_1 = 0.95$; $f_1 = 0.90$; $f_2 = 0.95$; $g_2 = -0.60$.)

small τ_o, becomes very important for large τ_o values (Fig. 6). The original collimated radiation, which is very important for optically thin samples, becomes negligible when compared to the scattered radiation, for optically thick samples. For small or medium τ_o values, the 'linear' model provides a good estimation of the normal scattered transmittance and, subsequently, of the optical thickness. However, it leads to an overestimation of this transmittance for large τ_o (Fig. 8). This overestimated value may be greater than the transmittance measured in the normal direction and a negative collimated transmittance is thus obtained, which is not realistic. The results given by the 'constant' and the 'second order' models are very similar for $2 < \tau_o < 15$. The later model gives results which are only 5% in error for $\tau_o = 20$. Globally it is the most accurate one, so it has been chosen for the direct determination of τ_o.

But this does not solve the entire identification problem. As a matter of fact, the sensitivity analysis showed that the sensitivity coefficients of g_1, g_2, f_1 and f_2 were almost linearly dependent. Numerical simulations showed that it was impossible to simultaneously determine the five remaining parameters. Since g_2 has the weakest sensitivity coefficient, which means that a variation of g_2 induces a smaller variation of the transmittances than the variations of the other parameters, it was left over during the estimation process. However, a preliminary choice of g_2 value is needed. This choice can be seen as a possibility to impose a specific form to the phase function as well suited as possible to the backscattering phenomena to be represented. Consequently, the following identification procedure is used: (i) a direct determination of the τ_o is carried out, using the 'second order' modification of the Beer's law model; (ii) g_2 is chosen; (iii) the Gauss linearization method is used to identify ω, g_1, f_1 and f_2.

7. EXPERIMENTAL RESULTS AND DISCUSSION

A critical problem for this kind of experiment is the lack of energy in off-normal scattering directions. This is due to the important attenuation introduced by the samples and to the necessity of operating with small solid angles, in order to preserve the angular resolution of the measurements. Despite the radiation source high temperature (a 1600°C blackbody furnace) it was necessary to operate with large monochromator slits. So the experimental set-up allowed us to cover the 0.5–5.5 μm wavelength band with a 1 μm spectral resolution. Thus the value of the parameters are given for the wavelength set 1, 2, 3, 4 and 5 μm. 86 kg m^{-3} density fiberglass insulation samples of 1.7, 2.3 and 4.0 mm thickness, have been tested as well as a 160 kg m^{-3} density composed sample (70% of silica fibers, 30% of cellulose) of thickness 0.3 mm. The characteristics of these samples are summarized in Tables 1 and 2. Transmittances have been measured for 11 directions and reflectances for 6 directions.

Figure 9 shows the optical thickness determined for the composed sample and for the 4 mm fiberglass sample. Even with the moderate resolution of the spectral measurements, the non-gray behavior of these materials can be observed. The scattering of the results is higher for the fiberglass sample, due to its high optical thickness value. Such scattering shows the limits of the experimental set-up for the transmittance measurements.

Figure 10 displays the fiberglass sample albedo ω and phase function parameters g_1, f_1 and f_2. Some variations with the wavelength are observed, with some dispersion in the data. This is a highly scattering material, with a forward concentration of scattering (high values of g_1, f_1 and f_2). The same parameters are shown in Fig. 11, for the composed sample. In this case the material is also a highly forward scattering

Table 1. Fiber diameter distribution for the fiberglass sample

$\phi[\mu m]$	10	12.5	15	17.5	20	22.5	25	30
%	2.5	7.5	35	15	15	17.5	5	2.5

Table 2. Fiber diameter distribution for the composed sample

$\phi[\mu m]$	0.5	1.5	2.5	3.5	4.5	5.5	6.5	7.5	8.5	9.5
%	34.5	15.1	7.3	5.9	4.2	5.4	6.1	5.7	3.6	3.1
$\phi[\mu m]$	10.5	11.5	12.5	13.5	14.5	15.5	16.5	17.5	18.5	19.5
%	2.5	1.9	1.6	1.1	0.6	0.5	0.3	0.1	0.2	0.2

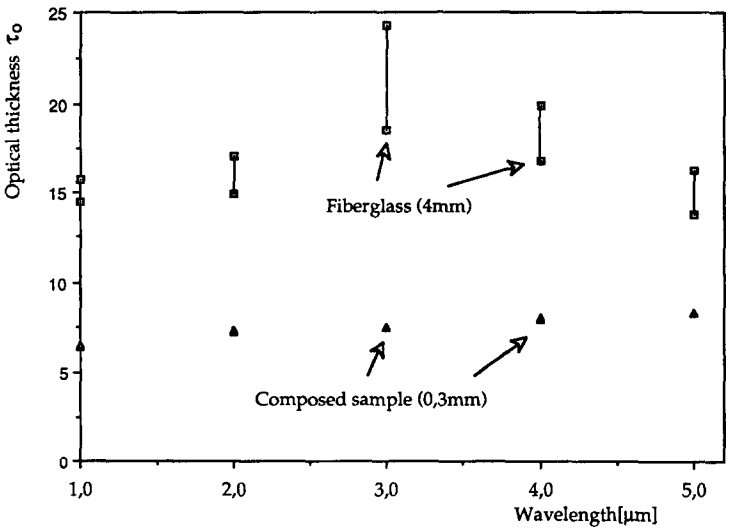

FIG. 9. Optical thickness for fiberglass (4.0 mm thick) sample and composed sample (0.3 mm thick).

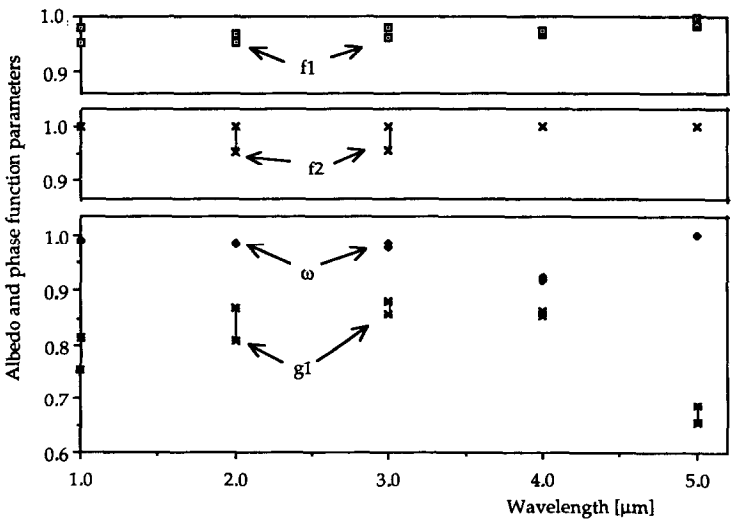

FIG. 10. Albedo and phase function parameters of fiberglass.

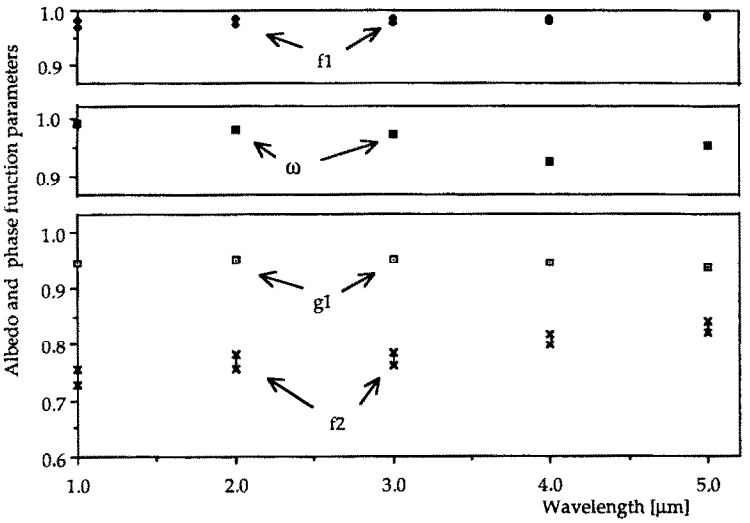

FIG. 11. Albedo and phase function parameters of silica fibers–cellulose composed sample.

one, with small differences in the parameters g_1 and f_2, compared to the fiberglass sample.

The parameter g_2 has been introduced in order to distinguish the shape of the backward and the forward scattering, but was not identified from the experimental values. The influence of g_2 on the objective function and on the other parameters are presented in Table 3. It shows that ω is sensitive to the choice of g_2, but the influence on the other parameters is very small. However there is a value which minimizes the root mean squared error. For the present case and for both type of materials, it corresponded to a g_2 value nearly equal to g_1. Since no prior information on the samples was available, it has been decided to choose $g_2 = g_1$.

Figure 12 presents the extinction coefficient vs the sample thickness, for the fiberglass samples. These samples were sliced in the same direction and in the same block of a material assumed to be homogenous. So the extinction coefficient should not depend on the sample thickness. For thin samples (1.7 and 2.3 mm), good results are obtained, but some scattering is observed for a 4 mm sample. As was already shown in Fig. 9, such scattering is a consequence of the high optical thickness value.

Theoretical and experimental transmittance as well as reflectance values for each discretized direction are compared in Fig. 13, for the composed sample and in Fig. 14, for the fiberglass sample. These plots represent two particular data series for a wavelength of 2 μm. In Fig. 13, for a rather moderate τ_0 value, the transmittances are more important than the reflectances. The collimated transmittance overpasses the scattered one in the normal direction. In Fig. 14, the opposite situation is observed. It corresponds to an optically thicker sample, for which the backscattered radiation is higher than the transmitted one. The transmittances are weak, becoming of the same order of magnitude

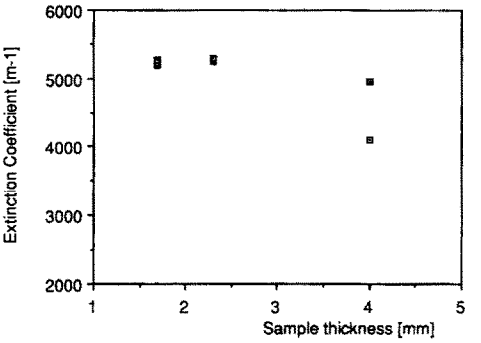

FIG. 12. Extinction coefficient vs sample thickness for fiberglass samples, $\lambda = 4$ μm.

Table 3. Influence of the parameter g_2 on the others parameters and on the root mean square error, for a fiberglass sample, ($\lambda = 3$ μm)

g_2	−0.50	−0.60	−0.70	−0.80	−0.90	−0.99
ω	0.98	0.98	0.98	0.98	0.98	0.98
g_1	0.92	0.92	0.91	0.89	0.88	0.88
f_1	0.93	0.95	0.97	0.97	0.98	0.98
f_2	1.00	0.97	0.96	0.97	0.98	0.98
$(1/N)\sqrt{[\Sigma(T_{ei}-T_{ti})^2]}$	1.75×10^{-3}	1.31×10^{-3}	8.84×10^{-4}	6.00×10^{-4}	5.20×10^{-4}	5.31×10^{-4}

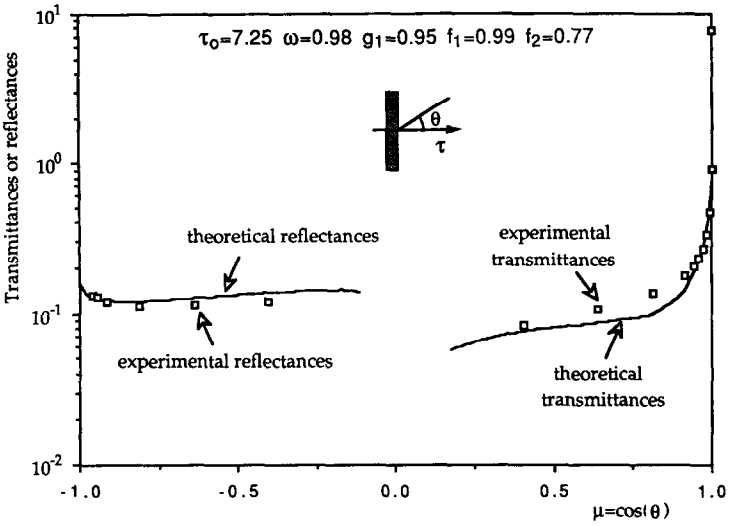

FIG. 13. Theoretical and experimental transmittances and reflectances values for the composed sample, ($\lambda = 2$ μm).

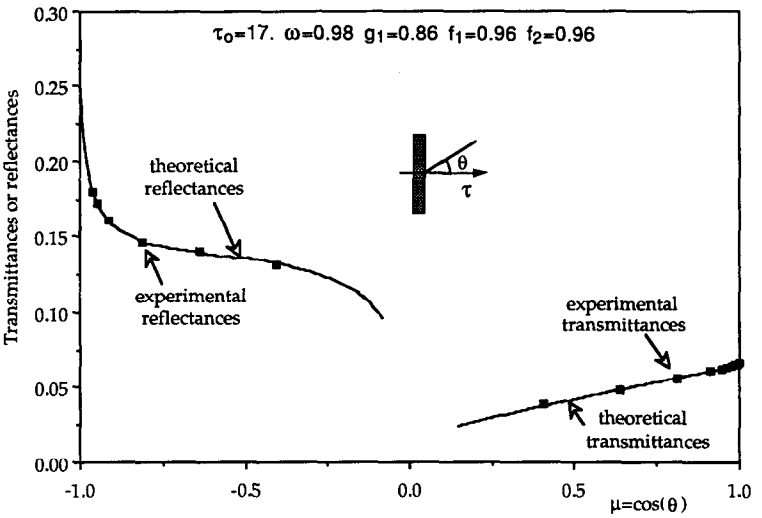

FIG. 14. Theoretical and experimental transmittances and reflectances values for the fiberglass sample, ($\lambda = 2$ μm).

as the measurement noise level. It is then difficult to determine τ_0 since its determination is based on the differences between the normal and the neighbor directions transmittances. However both cases show a good agreement between the experimental and the calculated values.

8. CONCLUSION

A parameter identification method based upon a sensitivity coefficient analysis has been presented. To our knowledge, this is a new approach in the area of the semi-transparent scattering materials characterization.

The sensitivity analysis has shown the difficulties of determining simultaneously the six unknown parameters. Such difficulties arise naturally from the choosen physical model, from the experimental collection of informations (number of measurement points and angular directions choice), and from the detector noise. However, it has been shown that a preliminary τ_0 determination by a direct method is a good approach. But, it still was not possible to estimate simultaneously the five remaining parameters. The one which has the smallest influence on the results had to be fixed, based on prior information. As a consequence the phase function model has been reduced to a three parameters model

and only four parameters have been simultaneously identified.

An optical thickness determination, instead of the extinction coefficient, is more adequate, since it allows comparisons between materials of different extinction coefficients and samples with different thicknesses. This identification is possible for optical thickness value smaller than 13 or 14 (depending on the other parameters). Therefore, the choice of a sample thickness for an experimentation depends on the material's extinction coefficient: it must be thin enough to obtain τ_0 under the above mentioned limit, but not too thin so as to be representative of the original material.

Future work will use a more sensitive detection device (FTIR spectrophotometer). It should improve the spectral resolution of the determined radiative properties as well as the identification process since many more measurements points will be available.

Acknowledgements—The first author was financially supported through a CNPq (Brazil)/SFERE-CEFI (France) Cooperation Fellowship, during this work.

REFERENCES

1. N. J. McCormick, Inverse radiative transfer problem: a review, *Proc. 12th International Transport Theory Conference* (1992) (in press).
2. V. A. Petrov, Inverse radiation problems in scattering semitransparent materials based on the radiation diffusion approximation, *Proc. 13th European Conference on Thermophysical Properties*, Lisbon (1993) (in press, *High Temp.–High Pressures*).
3. S. C. Lee, Scattering phase function for fibrous media, *Int. J. Heat Mass Transfer* **33,** 2183–2190 (1990).
4. D. Banner, S. Klarsfeld and C. Langlais, Temperature dependence on the optical characteristics of semi-transparent porous media, *High Temp.–High Pressures* **21,** 347–354 (1989).
5. G. Jeandel, P. Boulet and G. Morlot, Radiative transfer through a medium of silica fibers oriented in parallel planes, *Int. J. Heat Mass Transfer* **36,** 531–536 (1993).
6. H. Y. Yeh and J. A. Roux, Spectral radiative properties of fiberglass insulations, *J. Thermophys.* **2,** 78–81 (1989).
7. L. Glicksman, M. Schuetz and M. Sinofsky, Radiation heat transfer in foam insulation, *Int. J. Heat Mass Transfer* **30,** 187–197 (1987).
8. K. Kamiuto, M. Sato and M. Iwamoto, Determination of the radiative properties of high-porosity materials by use of the emerging-intensity fitting method, *J. Quant. Spectrosc. Radiat. Transfer* **42,** 477–482 (1989).
9. K. Kamiuto, M. Iwamoto, M. Sato and T. Nishimura, Radiation-extinction coefficients of packed-sphere systems, *J. Quant. Spectrosc. Radiat. Transfer* **45,** 93–96 (1991).
10. K. Kamiuto, M. Iwamoto, T. Nishimura and M. Sato, Albedo and asymmetry factors of the phase function for packed-sphere systems, *J. Quant. Spectrosc. Radiat. Transfer* **46,** 309–316 (1991).
11. K. Kamiuto, Application of the emerging-intensity fitting method for inverse scattering problems to a system bounded by transparent plates, *J. Quant. Spectrosc. Radiat. Transfer* **46,** 159–164 (1991).
12. J. Kuhn, S. Korder, M. C. Arduini-Schuster, G. Göbel and J. Fricke, Infrared-optical properties of insulating powders, *Proc. 13th European Conference on Thermophysical Properties*, Lisbon, 1993 (in press, *High Temp.–High Pressures*).
13. J. F. Sacadura, G. Uny and A. Venet, Models and experiments for radiation parameter estimation of absorbing, emitting and anisotropically scattering media, *8th Int. Heat Transfer Conference*, Vol. 2, pp. 565–570. San Francisco (1986).
14. G. Uny, Modélisation du transfert couplé rayonnement-convection au sein de matériaux poreux et identification de leurs propriétés radiatives: application aux laines de verre, Doctoral Thesis no 86 ISAL 0007, INSA, Lyon, France (1986).
15. J. F. Sacadura and V. P. Nicolau, Spectral radiative properties identification of semi-transparent porous media, *3rd UK National & 1st European Conference in Thermal Sciences*, Birmingham, UK, pp. 717–723 (1992).
16. F. Doumenc, Détermination des propriétés radiatives des milieux poreux—Application aux laines de verre, DEA rapport, INSA-CETHIL, Lyon, France (1989).
17. J. V. Beck and K. J. Arnold, *Parameter Estimation in Engineering and Science*. Wiley, New York (1977).
18. E. Hensel, *Inverse Theory and Applications for Engineers*, Chap. 2. Prentice-Hall, Englewood Cliffs, NJ (1991).